PROCEEDINGS OF SCIENCE

Photon and dilepton production rate in the quark-gluon plasma from lattice QCD

Harvey B. Meyer,[a,b,e,*] **Marco Cè,**[c] **Tim Harris,**[d] **Ardit Krasniqi**[a] **and Csaba Török**[a]

[a] *PRISMA$^+$ Cluster of Excellence and Institute for Nuclear Physics, Johannes Gutenberg University Mainz, 55099 Mainz*

[b] *Helmholtz Institute Mainz, Johannes Gutenberg University Mainz, 55099 Mainz*

[c] *Albert Einstein Center for Fundamental Physics (AEC) and Institut für Theoretische Physik, Universität Bern, Sidlerstrasse 5, CH-3012 Bern, Switzerland*

[d] *School of Physics and Astronomy, University of Edinburgh, EH9 3JZ, United Kingdom*

[e] *GSI Helmholtzzentrum für Schwerionenforschung, 64291 Darmstadt, Germany*

E-mail: meyerh@uni-mainz.de

The photon emissivity of the quark-gluon plasma (QGP) is an important input to predict the photon yield in heavy-ion collisions, particularly for transverse momenta in the range of 1 to 2 GeV. Photon production in the QGP can be probed non-perturbatively in lattice QCD via (Euclidean) time-dependent correlators. Analyzing the spatially transverse channel, as well as the difference of the transverse and longitudinal channels as a consistency check, we determine the photon emissivity based on continuum-extrapolated correlators in two-flavour QCD. Estimates of the lepton-pair production rate can be derived by combining the two aforementioned channels.

The 39th International Symposium on Lattice Field Theory,
8th-13th August, 2022,
Rheinische Friedrich-Wilhelms-Universität Bonn, Bonn, Germany

*Speaker

PoS(LATTICE2022)186

1. Introduction

The primary goals of high-energy heavy-ion collisions is to produce and study the quark-gluon plasma (QGP), the high-temperature phase of QCD. As any thermal medium containing charged particles, the QGP radiates photons. Since the emission of a real photon by a quasiparticle is only kinematically possible if it collides with another constituent of the medium, the photon emissivity is directly sensitive to interactions in the medium.

In a heavy-ion collision, the direct photons, i.e. those not produced via hadronic decays in the final stage of the reaction, encode information about the environment in which they were created; see the reviews [1, 2]. At transverse momentum $1 \lesssim p_T/\mathrm{GeV} \lesssim 3$, one expects a sizeable contribution from thermal photons, both from the QGP and from the hadronic phase. At RHIC, with a center-of-mass energy per nucleon of $\sqrt{s_{NN}} = 200\,\mathrm{GeV}$, the PHENIX measurement of $p_T < 3\,\mathrm{GeV}$ photons showed a clear excess over N_{coll}-scaled pp measurement [3] (see also the more recent preprint [4]). Furthermore, the same experiment found a large photon anisotropy with respect to the reaction plane [5]. However, the STAR collaboration [6] obtained a smaller photon yield than PHENIX, a tension that remains to be understood. At the LHC with $\sqrt{s_{NN}} = 2760\,\mathrm{GeV}$, ALICE measured the photon yield [7] as well as the photon elliptic flow [8]. For a recent comparison of predictions based on the hydrodynamic modelling of heavy-ion collisions to experimental measurements of direct photons, see [9].

Here our goal is to compute the photon emissivity of the QGP at temperatures reached in heavy-ion collisions from first principles. The thermal vector spectral functions are defined as the Fourier transforms of the commutators of electromagnetic currents,

$$\rho^{\mu\nu}(\mathcal{K}) = \int d^4x\, e^{i\mathcal{K}\cdot x}\, \frac{1}{Z} \sum_n e^{-E_n/T} \langle n|[j^\mu(x), j^\nu(0)]|n\rangle,$$

with the $|n\rangle$ being energy eigenstates of eigenvalue E_n and $Z = \sum_n e^{-E_n/T}$ the canonical partition function. The physical significance of these spectral functions is illustrated by the following relations to electromagnetic observables [10]. The rate of photon emission per unit volume plasma is given at leading order by ($\mathcal{K} \equiv (\omega, \vec{k})$ and $k \equiv |\vec{k}|$)

$$d\Gamma_\gamma(k) = \alpha\, \frac{d^3k}{4\pi^2\, k}\, \frac{-\rho^\mu{}_\mu(\omega = k, \vec{k})}{e^{\beta k} - 1}. \tag{1}$$

Similarly, the dilepton production rate (via a timelike photon) is given at leading order by

$$d\Gamma_{\ell^+\ell^-}(\mathcal{K}) = \alpha^2\, \frac{d^4\mathcal{K}}{6\pi^3\mathcal{K}^2}\, \frac{-\rho^\mu{}_\mu(\mathcal{K})}{e^{\beta\omega} - 1}\,. \tag{2}$$

In Eq. (2), the four-vector $\mathcal{K}$ must obviously be timelike, and $\mathcal{K}^2 = M_{\ell\ell}^2$ then corresponds to the invariant mass squared of the lepton pair. By contrast, in Eq. (1) the four-vector $\mathcal{K}$ is lightlike. The regime of spacelike virtualities, $\mathcal{K}^2 < 0$, though of less direct phenomenological relevance, is interesting in its own right, as it describes the ability of the medium to absorb the energy stored in external electromagnetic fields and turn it into heat [10–12].

In lattice QCD, which is based on the imaginary-time path-integral representation of QFT (Matsubara formalism), the vector correlators ($\{\gamma^\mu, \gamma^\nu\} = 2g^{\mu\nu} = 2\mathrm{diag}(1,-1,-1,-1)$),

$$G^{\mu\nu}(x_0, \vec{k}) = \int d^3x\, e^{-i\vec{k}\cdot\vec{x}}\, \mathrm{Tr}\Big\{\frac{e^{-\beta H}}{Z(\beta)} j^\mu(x)\, j^\nu(0)\Big\}, \qquad j^\mu = \sum_f Q_f\, \bar{\psi}_f \gamma^\mu \psi_f \tag{3}$$

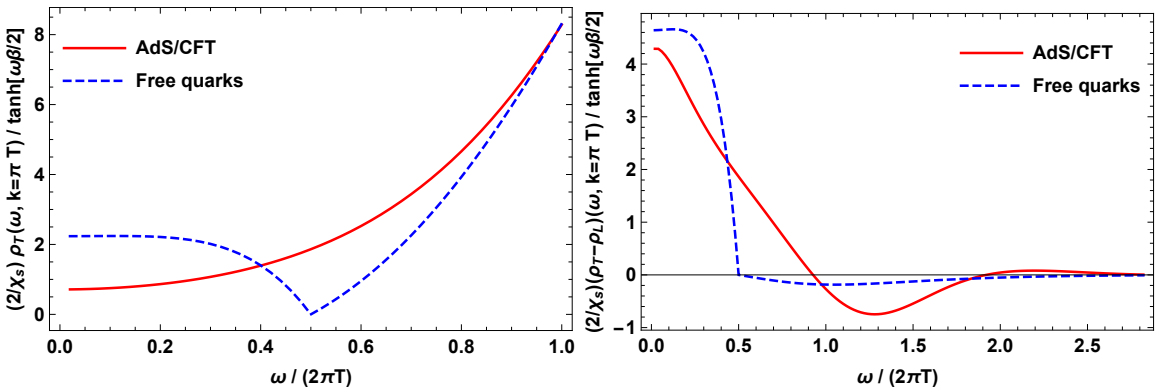

Figure 1: Illustration of the transverse (left) and transverse-minus-longitudinal channels (right) for $k = \pi T$ in the theory of non-interacting quarks (see e.g. [13]) and the strongly-coupled $\mathcal{N} = 4$ super-Yang-Mills theory in the limit of a large number of colours. In the latter case, the spectral functions are obtained via the AdS/CFT correspondence [14]. The static susceptibility $\chi_s \equiv \int d^4x \langle j^0(x) j^0(0)\rangle$ provides a natural normalization to compare different theories.

can be computed, with $j^\mu(x) = e^{x_0 H - i\vec{x}\cdot\vec{P}} j^\mu(0) e^{-x_0 H + i\vec{x}\cdot\vec{P}}$. They are related via the spectral representation to the spectral functions introduced above,

$$u_\mu G^{\mu\nu} u_\nu(x_0, \vec{k}) = \int_0^\infty \frac{d\omega}{2\pi} \underbrace{\frac{(u_\mu \rho^{\mu\nu} u_\nu)(\omega, \vec{k})}{\sinh(\beta\omega/2)}}_{\geq 0} \cosh[\omega(\beta/2 - x_0)], \tag{4}$$

where u is a real four-vector. Determining the spectral function from the Euclidean correlators is a mathematically well-defined, but numerically ill-posed problem.

2. A choice of basis for $\rho^{\mu\nu}$

The current-conservation relation $\omega^2 \rho^{00}(\omega, k) = k^i k^j \rho^{ij}(\omega, k)$ implies that the longitudinal component

$$\rho_L \equiv (\hat{k}^i \hat{k}^j \rho^{ij} - \rho^{00}) = \frac{\mathcal{K}^2}{k^2} \rho^{00} \tag{5}$$

vanishes at real-photon kinematics, $\mathcal{K}^2 = 0$. Note that we use the notation $k \equiv |\vec{k}|$ and $\hat{k}^i = k^i/k$. Defining the transverse component as

$$\rho_T \equiv \frac{1}{2}(\delta^{ij} - \hat{k}^i \hat{k}^j)\rho^{ij} \tag{6}$$

and introducing the linear combination ($\lambda \in \mathbb{R}$)

$$\rho(\omega, k, \lambda) = 2\rho_T + \lambda\, \rho_L\,, \tag{7}$$

it is clear that $\rho(\omega, k, 1) = -\rho^\mu{}_\mu(\omega, \vec{k})$. Thus $-\rho^\mu{}_\mu$ can be replaced by $\rho(\omega, k, \lambda)$ for any value of λ on the right-hand side of Eq. (1).

Two channels appear most promising in face of the inverse problem that needs to be overcome; see Fig. 1. The channel $2(\rho_T - \rho_L)$, which corresponds to $\lambda = -2$ and vanishes in the vacuum

label	$(6/g_0^2, \kappa)$	$1/(aT)$	N_{conf}	$\frac{\mathrm{MDUs}}{\mathrm{conf}}$
F7	$(5.3, 0.13638)$	12	482	20
O7	$(5.5, 0.13671)$	16	305	20
W7	$(5.685727, 0.136684)$	20	1566	8
X7	$(5.827160, 0.136544)$	24	511	10

Table 1: Table of $N_f = 2$ gauge ensembles at temperature $T \simeq 250\,\mathrm{MeV}$ and aspect ratio $LT = 4$ at four different lattice spacings. The number of available configurations and the amount of Monte-Carlo time separating successive configurations is indicated in the last two columns.

due to Lorentz symmetry, is highly suppressed at large ω and thereby obeys a superconvergent sum rule [11]. Secondly, the transverse-channel spectral function ρ_T, corresponding to $\lambda = 0$, is positive-definite and free of the diffusion pole; we have studied this channel in a recent lattice calculation [15]. Finally, denoting the static susceptibility by $\chi_s = \int d^4x \langle j^0(x) j^0(0) \rangle$, we note that the 'effective diffusion coefficient'

$$D_{\mathrm{eff}}(k) \equiv \frac{\rho(\omega = k, k, \lambda)}{4\chi_s k} \tag{8}$$

is a useful quantity [16] to compare the photon emissivity of theories with different numbers of degrees of freedom.

3. $N_f = 2$ lattice calculations at $T \simeq 250\,\mathrm{MeV}$

We employ $N_f = 2$ flavours of dynamical O(a) improved Wilson fermions with the Wilson gauge action (see e.g. [17]). The simulations are based on the openQCD code [18]. The aspect ratio is fixed to $L \cdot T = 4$, corresponding to $L \simeq 3.1\,\mathrm{fm}$. Four ensembles with lattice spacings between 0.032 and 0.064 fm are used to extrapolate the vector correlators to the continuum; see Table 1. With the parameters of ensembles F7 and O7, the zero-temperatre pion mass is about 270 MeV [17]. We focus on the two-point function of the isovector current $j^\mu = \frac{1}{\sqrt{2}}(\bar{u}\gamma^\mu u - \bar{d}\gamma^\mu d)$. In particular, we obtained for the static susceptibility [15]

$$\chi_s / T^2 = 0.882(11)_{\mathrm{stat}}(19)_{\mathrm{syst}}, \tag{9}$$

where we quote the statistical error and the systematic error of the continuum extrapolation.

3.1 The transverse-minus-longitudinal channel

Beginning with the analysis of $\rho(\omega, k, \lambda = -2) = 2(\rho_T - \rho_L)$ [11], we note that the correlator could be obtained in the continuum at seven equidistant points in the range $0.25 \leq T x_0 \leq 0.50$ with an uncertainty of one to two permille. The spectral function $\rho(\omega, k, -2)$ is non-negative for $\omega \leq k$, and the operator-product expansion (OPE) predicts that $\rho(\omega, k, -2) \sim k^2/\omega^4$ as $\omega \to \infty$, from where the superconvergent sum rule

$$\int_0^\infty d\omega\, \omega\, \rho(\omega, k, -2) = 0 \tag{10}$$

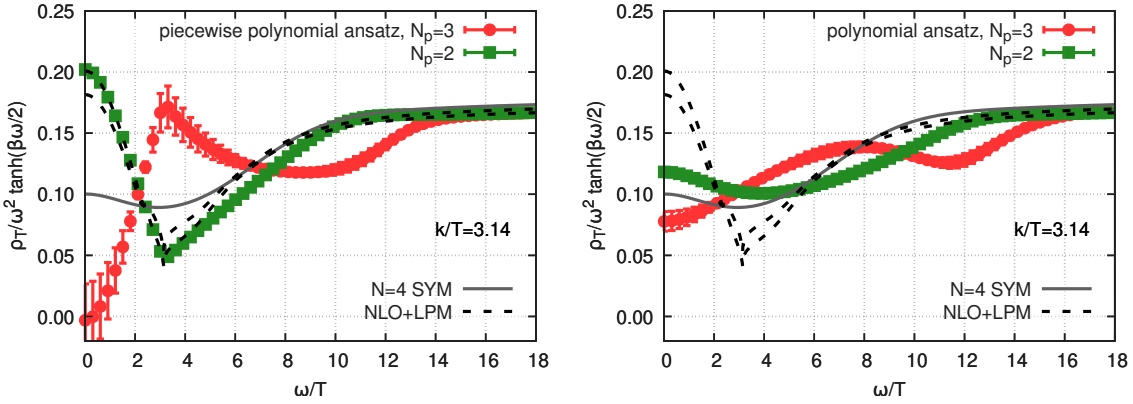

Figure 2: Transverse-channel spectral function at $k = \pi T$: results from fitting the polynomial and piecewise-polynomial ansätze with either two or three free parameters. For comparison, the NLO weak-coupling [19, 20] and the AdS/CFT prediction [14] are displayed as dashed and full curves, respectively.

follows. Motivated by the 'hydrodynamics' prediction at small ω, k characterized by the diffusion pole, we are led to the five-parameter ansatz

$$\rho(\omega, k, -2) = \frac{A(1 + B\omega^2)\ \tanh(\omega\beta/2)}{[(\omega - \omega_0)^2 + b^2][(\omega + \omega_0)^2 + b^2][\omega^2 + a^2]}. \tag{11}$$

The analysis strategy in [11] consisted in locally parametrizing the k-dependence of the 'non-linear' parameters (a, b, ω_0) and scanning over these to determine the χ^2 landscape; the parameter B is always determined so as to satisfy the sum rule (10), and A by exact minimization of the χ^2 at given (a, b, ω_0). In spite of the high precision of the correlator, the form of the spectral function remains poorly constrained at low k. The predictivity improves notably at $k > \pi T$. In this way, we obtained an upper bound on $D_{\text{eff}}(k)$, which is displayed as a dotted line in Fig. 3. A point worth mentioning is that the ansatz used only allows for one zero of $\rho(\omega, k, -2)$ viewed as a function of ω, whereby $\rho(\omega, k, -2)$ tends to zero from below as $\omega \to \infty$. However, it was subsequently shown via a next-to-leading calculation [19] that $\rho(\omega, k, -2)$ asymptotically approaches zero from above, i.e. $\rho(\omega, k, -2)$ must have at least two zero-crossings. In the future, it could be worth returning to the analysis of the $(T - L)$ channel, with smaller lattice spacings giving access to smaller x_0, and taking into account the additional structure of $\rho(\omega, k, -2)$ at high ω.

3.2 The transverse channel

In [15], the continuum limit of the lattice correlators was taken point-by-point in x_0 from the available four lattice spacings and three discretizations of the vector correlator. Allowing for cuts to the data as well as extending the fit ansatz beyond the standard form linear in a^2, the full uncertainty of the continuum-extrapolated correlator is obtained using the Akaike information criterion, including an estimate of the systematic error. It is this extrapolated set of between six and nine correlator points that enters the fits for the spectral function.

The chosen fit ansatz for the spectral function reads

$$\rho(\omega) = \rho_{\text{fit}}(\omega)(1 - \Theta(\omega, \omega_0, \Delta)) + \rho_{\text{pert}}(\omega)\Theta(\omega, \omega_0, \Delta),$$

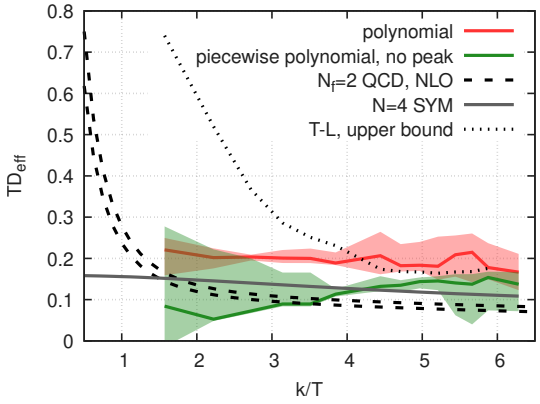

Figure 3: Results for the effective diffusion constant $D_{\rm eff}(k)$ from the analysis of the transverse channel with the polynomial and the piecewise-polynomial ansatz. The upper limit obtained from the $(T-L)$ channel analysis is shown as a dotted line. Combining the information from the two channels improves the predictivity on $D_{\rm eff}(k)$. For comparison, the leading-order weak-coupling results [21] and the strongly-coupled $\mathcal{N}=4$ SYM [14] results are displayed as dashed and solid lines, respectively.

with $\omega_0 = 2.5\ldots3.0\,\mathrm{GeV}$ being the matching frequency, $\Theta(\omega,\omega_0,\Delta) = (1+\tanh[(\omega-\omega_0)/\Delta])/2$ a smooth step function and $\rho_{\rm pert}(\omega)$ is taken from the NLO calculation [19]. Either the polynomial ansatz

$$\frac{\rho_{\rm fit,1}(\omega)}{T^2} = \sum_{n=0}^{N_{\rm p}-1} A_n \left(\frac{\omega}{\omega_0}\right)^{1+2n},$$

or the piecewise polynomial ansatz was chosen,

$$\frac{\rho_{\rm fit,2}(\omega)}{T^2} = \begin{cases} A_0\,\dfrac{\omega}{\omega_0} + A_1\left(\dfrac{\omega}{\omega_0}\right)^3, & \text{if } \omega \le k, \\ B_0\,\dfrac{\omega}{\omega_0} + B_1\left(\dfrac{\omega}{\omega_0}\right)^3, & \text{if } \omega > k, \end{cases}$$

where continuity is enforced at $\omega = k$. The former ansatz is motivated by the form of the strongly coupled $\mathcal{N}=4$ SYM spectral functions, while the latter is able to reproduce the kink found at weak coupling (see the left panel of Fig. 1). Some representative results of the fitting procedure are shown in Fig. 2. The piecewise polynomial ansatz with three fit parameters led in some cases to fit results with a maximum at $\omega = k$, rather than the minimum expected from the weak-coupling spectral function. For $k \gtrsim \pi T$, such results are strongly disfavoured by the data on the $(T-L)$ channel, however. Thus, restricting the fitted spectral functions to having a minimum within one standard deviation, one arrives at the results displayed in Fig. 3.

3.3 The dilepton rate

From the two channels analyzed above, the linear combination required to predict the dilepton production rate can be obtained according to

$$-\rho^{\mu}{}_{\mu} = 3\rho_T - (\rho_T - \rho_L). \tag{12}$$

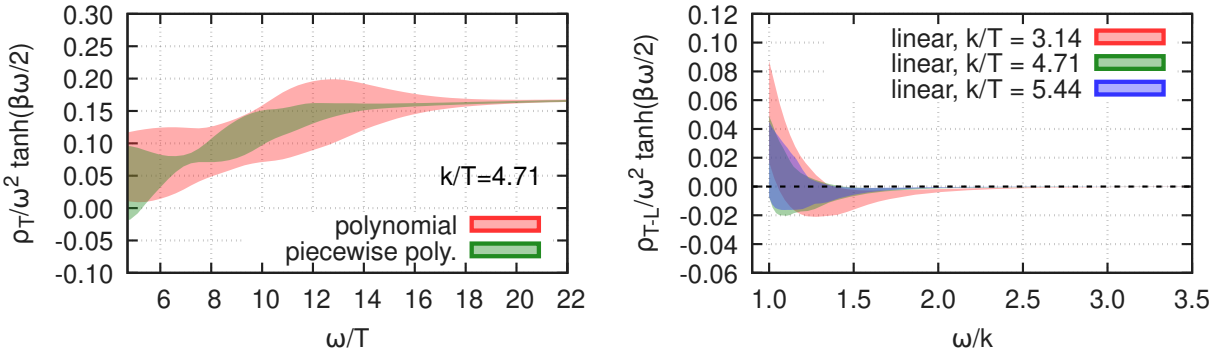

Figure 4: Comparison of the two channels contributing in Eq. (12) to the linear combination $-\rho^{\mu}{}_{\mu}$ relevant for the dilepton production rate. For orientation on the left panel, the free-quark prediction is $\rho_T \tanh(\omega\beta/2)/\omega^2 = 0.093$ at $\omega = 7.85T$.

Choosing for instance the spatial momentum $k = 4.71T = 1.2\,\text{GeV}$, a dilepton mass of $M_{\ell\ell} = 2\pi T = 1.6\,\text{GeV}$ corresponds to a frequency of $\omega = (M_{\ell\ell}^2 + k^2)^{1/2} = 7.85T = 1.67k = 2.0\,\text{GeV}$. For that frequency, from the left panel of Fig. 4 one reads off that $\rho_T \tanh(\omega\beta/2)/\omega^2$ lies between 0.05 and 0.13, while the right panel shows that $-0.01 \lesssim (\rho_T - \rho_L)\tanh(\omega\beta/2)/\omega^2 \lesssim 0.0$. Thus we see that the term $3\rho_T$ in Eq. (12) strongly dominates. More generally, this term is three times larger than the second one at $M_{\ell\ell} = 0$ (since ρ_L vanishes at this kinematic point), and becomes rapidly more dominant as the dilepton mass is increased.

4. Conclusion

Starting from continuum-extrapolated Euclidean correlators computed on the lattice, we have analyzed two independent spectral functions, ρ_T and $(\rho_T - \rho_L)$, that fully determine the thermal polarization tensor. The analysis is based on the spectral representation of the correlators at fixed spatial momentum k and requires solving a numerically ill-posed inverse problem. We have approached this problem by employing fit ansätze capable of describing in a satifactory manner both the next-to-leading order weak-coupling spectral functions and those of the strongly-coupled $\mathcal{N} = 4$ super-Yang-Mills theory. The complementary analysis of two different channels provided an important cross-check at photon kinematics ($\omega = k$), where ρ_L vanishes and allowed us to better constrain the photon emissivity than from one channel alone.

We find that our lattice results are consistent with the LO weak-coupling prediction. However, our results in the range $1 \lesssim k[\text{GeV}] \lesssim 1.4$ can also accomodate a photon emissivity three times larger than the LO prediction. This observation is interesting in light of the phenomenological situation sketched in the introduction, given in particular the high photon yield measured by the PHENIX experiment at RHIC.

The available data allows us to make predictions for the dilepton rate (see Eq. (2)) by combining the two analyzed channels according to Eq. (12). In the latter linear combination, the transverse channel increasingly dominates as the dilepton mass is increased. At this point, the dilepton rate deriving from the lattice data is consistent within uncertainties with the leading-order (free-quark) perturbative prediction.

An alternative way to probe the photon emissivity of the QGP on the lattice is to compute correlation functions at vanishing virtuality, by injecting an imaginary spatial momentum [22, 23]. First results have been reported at this conference [24].

We thank Arianna Toniato for a fruitful and enjoyable collaboration. This work was supported by the European Research Council (ERC) under the European Union's Horizon 2020 research and innovation program through Grant Agreement No. 771971- SIMDAMA, as well as by the Deutsche Forschungsgemeinschaft (DFG, German Research Foundation) through the Cluster of Excellence "Precision Physics, Fundamental Interactions and Structure of Matter" (PRISMA+ EXC 2118/1) funded by the DFG within the German Excellence strategy (Project ID No. 39083149).

References

[1] G. David, Rept. Prog. Phys. **83**, 046301 (2020), arXiv:1907.08893.
[2] F. Geurts and R.-A. Tripolt, Prog. Part. Nucl. Phys. **128**, 104004 (2023), arXiv:2210.01622.
[3] PHENIX, A. Adare *et al.*, Phys. Rev. Lett. **104**, 132301 (2010), arXiv:0804.4168.
[4] PHENIX, U. A. Acharya *et al.*, (2022), arXiv:2203.17187.
[5] PHENIX, A. Adare *et al.*, Phys. Rev. Lett. **109**, 122302 (2012), arXiv:1105.4126.
[6] STAR, L. Adamczyk *et al.*, Phys. Lett. B **770**, 451 (2017), arXiv:1607.01447.
[7] ALICE, J. Adam *et al.*, Phys. Lett. B **754**, 235 (2016), arXiv:1509.07324.
[8] ALICE, S. Acharya *et al.*, Phys. Lett. B **789**, 308 (2019), arXiv:1805.04403.
[9] C. Gale, J.-F. Paquet, B. Schenke, and C. Shen, Phys. Rev. C **105**, 014909 (2022), arXiv:2106.11216.
[10] L. D. McLerran and T. Toimela, Phys.Rev. **D31**, 545 (1985).
[11] M. Cè, T. Harris, H. B. Meyer, A. Steinberg, and A. Toniato, Phys. Rev. D **102**, 091501 (2020), arXiv:2001.03368.
[12] M. Cè, T. Harris, H. B. Meyer, and A. Toniato, JHEP **03**, 035 (2021), arXiv:2012.07522.
[13] M. Laine, JHEP **1311**, 120 (2013), arXiv:1310.0164.
[14] S. Caron-Huot, P. Kovtun, G. D. Moore, A. Starinets, and L. G. Yaffe, JHEP **0612**, 015 (2006), arXiv:hep-th/0607237.
[15] M. Cè, T. Harris, A. Krasniqi, H. B. Meyer, and C. Török, Phys. Rev. D **106**, 054501 (2022), arXiv:2205.02821.
[16] J. Ghiglieri, O. Kaczmarek, M. Laine, and F. Meyer, Phys. Rev. **D94**, 016005 (2016), arXiv:1604.07544.
[17] P. Fritzsch *et al.*, Nucl.Phys. **B865**, 397 (2012), arXiv:1205.5380.
[18] http://luscher.web.cern.ch/luscher/openQCD (2013).
[19] G. Jackson and M. Laine, JHEP **11**, 144 (2019), arXiv:1910.09567.
[20] G. Jackson, Phys. Rev. D **100**, 116019 (2019), arXiv:1910.07552.
[21] P. B. Arnold, G. D. Moore, and L. G. Yaffe, JHEP **0112**, 009 (2001), arXiv:hep-ph/0111107.
[22] H. B. Meyer, Eur. Phys. J. **A54**, 192 (2018), arXiv:1807.00781.
[23] H. B. Meyer, M. Cè, T. Harris, A. Toniato, and C. Török, PoS **LATTICE2021**, 269 (2022), arXiv:2112.00450.
[24] C. Török *et al.*, Estimation of the photon production rate using imaginary momentum correlators, in *39th International Symposium on Lattice Field Theory*, 2022, arXiv:2212.05622.